
Article:
Babiker, Mohamed orcid.org/0000-0003-0659-5247, Koksal, Koray, Lembessis, V. E. et al. (1 more author) (2021) Chirality and helicity of linearly-polarised Laguerre-Gaussian beams of small beam waists. Optics Communications. 126907. ISSN 0030-4018

https://doi.org/10.1016/j.optcom.2021.126907

Chirality and helicity of linearly-polarised Laguerre-Gaussian beams of small beam waists

K. Koksal*+, M. Babiker
*Department of Physics, University of York, YO10 5DD, UK and
+Physics Department, Bitlis Eren University, Bitlis 13000, Turkey

V. E. Lembessis
Quantum Technology Group, Department of Physics and Astronomy,
College of Science, King Saud University, Riyadh 11451, Saudi Arabia

J. Yuan
Department of Physics, University of York, YO10 5DD, UK
(Dated: March 23, 2021)

The chirality and helicity of a linearly polarised Laguerre-Gaussian (LG) beam are examined. Such a type of light possesses a large longitudinal field amplitude when it is created with a sufficiently small beam waist and so gives rise to substantial magnitudes of chirality and helicity density distributions. In the simplest case of a doughnut beam of winding number $\ell = 1$ and another identical to it but for which $\ell = -1$, we obtain different chirality and helicity distributions in the focal plane $z = 0$. We also show that this chiral behaviour persists and the patterns evolve so that on planes at $z < 0$ and $z > 0$ the beam convergence phase contributes differently to the changes in the chirality and helicity distributions.

PACS numbers: 42.25.Ja; 33.55.+b; 78.20.Ek

Recent developments in the generation of laser light beams have highlighted the advances in the ability to focus light to sub-wavelength dimensions [1–4]. Light fields such as Laguerre-Gaussian (LG) beams possess a new feature, namely that the longitudinal (axial) component of the vortex electric field, which is normally regarded as insignificant, now acquires a magnitude comparable to the transverse components.

Some phenomena have been identified as consequences of strongly focused light such as LG beams, including novel field distributions [5, 6], modifications of the spin-orbit interaction [7, 8], the creation of transverse orbital angular momentum components [9–12] and changes in the interaction of light with matter [13]. The recent experimental report by Wozniak et al [14] demonstrated that this type of strongly focused light, although linearly-polarised and so has zero optical spin, exhibits a chiral behaviour [8] in the sense that it involves distinguishing between beams with equal but different signs of the winding number ℓ. In other words, it is not possible by rotation alone to superimpose the chirality distribution for ℓ on that for $-\ell$. Note that in this type of strongly focused light the LG beam itself is subject to a focusing lens and in the experiment by Wozniak et al [14] the fields arise due to vectorial diffraction processes and its chirality was observed at the lens focal plane,

This paper is concerned with a different type of focused light, namely that involving the electromagnetic fields of linearly polarised LG beams created with sufficiently small beam waists and not subject to vectorial diffraction. Our aim is to evaluate the chirality and the helicity distributions of such light beams, which are linearly-polarised and so have no optical spin, both in and in the vicinity of the focal plane. The evaluations depend on incorporating two ingredients. The first ingredient involves the inclusion of the longitudinal field component which we show is substantial only when the beam waist is sufficiently small. The second involves taking full account of the convergence phase embodied in the Gouy and curvature phases and the variations of the beam waist with the axial coordinate. In such beams the gradients of the convergence phases and that of the z-dependence of the beam waist $w(z)$ play significant roles in the chirality and helicity distributions in the vicinity and on either sides of the focal plane.

For simplicity we consider the first two doughnut modes for each of which the radial index $p = 0$. These have the same magnitudes but different signs of the winding number $\ell = \pm 1$. Both are taken to be linearly-polarised, so neither has optical spin and, without loss of generality, we take the linear polarisation vector to lie along the x-axis. For $\ell = \pm 1$ the electric field can be written in cylindrical coordinates $\mathbf{r} = (\rho, \phi, z)$ in terms of the amplitude function $U_{k10}(\rho, z)$ for $\ell = 1$. This amplitude function is exactly the same as $U_{k(-1)0}(\rho, z)$ for $\ell = -1$. The respective phase functions differ, however. In the paraxial approximation we have for the amplitude functions [15, 16]

$$E^x_{k\ell 0}(\mathbf{r}) = U_{k\ell 0}(\rho, z) e^{i\Theta_{k\ell 0}(\mathbf{r})} \tag{1}$$

where $\ell = \pm 1$ and the superscript x in E^x indicates wave polarisation along the x-axis. A Laguerre-Gaussian light

beam linearly-polarised along x is justifiable in the paraxial approximation [17] and has been adopted widely in such contexts. The amplitude functions for $\ell = \pm 1$ are identical and are given by

$$U_{k\pm 10}(\rho, z) = \mathcal{U}_0 \frac{1}{(1 + z^2/z_R^2)^{1/2}} \Big(\frac{\rho\sqrt{2}}{w(z)}\Big) e^{-\frac{\rho^2}{w(z)^2}}. \quad (2)$$

In the above $\mathcal{U}_0$ is a normalisation factor such that the total power of the beam is a constant which is specified below; $w(z)$ is the beam waist at axial coordinate z such that $w^2(z) = 2(z^2 + z_R^2)/kz_R$, where z_R is the Rayleigh range, $w_0 = w(0)$ is the beam waist at the focal plane $z = 0$. The phase functions of the doughnut modes including the convergence phases are as follows

$$\Theta_{k\pm 10}(\mathbf{r}) = kz \pm \phi + \theta_{Gouy} + \theta_{curve} \quad (3)$$

where θ_{Gouy} and θ_{curve} are given by

$$\theta_{Gouy} = -2\tan^{-1}(z/z_R); \quad \theta_{curve} = \frac{k\rho^2 z}{2(z^2 + z_R^2)}, \quad (4)$$

Note that these convergence phases vanish at the focal plane, but have different variations in the planes $z > 0$ and $z < 0$ on either side of the focal plane. The above electric field functions of a linearly-polarised paraxial doughnut mode of winding number ℓ arises directly from the non-paraxial theory [18] on taking the parxial limit.

In addition to the transverse component of the electric field given in Eq.(1) there must also exist a longitudinal (or axial) component E^z. This is because the total electric field vector $\mathbf{E}$ must satisfy the transversality condition $\boldsymbol{\nabla} \cdot \mathbf{E} = 0$ where

$$\mathbf{E} = E^x \hat{\boldsymbol{x}} + E^z \hat{\boldsymbol{z}} \quad (5)$$

Here carets indicate unit vectors. The axial component E^z follows formally from the transversality condition and is in a closed analytical form as follows

$$E^z_{k10}(\mathbf{r}) = -i\mathcal{U}_0 \left(\frac{4\rho^2 \cos\phi - w(z)^2 e^{-i\phi}}{Qkw(z)^4}\right) \times e^{-\frac{\rho^2}{w(z)^2} + i\Theta_{k10}} \quad (6)$$

where $Q = \sqrt{k/4z_R}$. The overall normalisation factor $\mathcal{U}_0$ appearing in Eqs.(2) and (6) is such that the power of the beam P is conserved. We have

$$\mathcal{U}_0^2 = \frac{P}{\frac{1}{2}\epsilon_0 c \int_0^{2\pi} \int_0^{\infty} \tilde{\mathbf{E}}_{k10} \cdot \tilde{\mathbf{E}}^*_{k10} \rho d\rho d\phi} \quad (7)$$

where the components of $\tilde{\mathbf{E}}_{k10}$ are $\tilde{E}^x_{k10}$ and $\tilde{E}^z_{k10}$.

$$\int_0^{2\pi} \int_0^{\infty} \tilde{\mathbf{E}}_{k10} \cdot \tilde{\mathbf{E}}^*_{k10} \rho d\rho d\phi = \frac{\pi w_0^2 \left(6 + k^2 w(z)^2\right)}{2k^2 w(z)^2} \quad (8)$$

From Eq.(6) it is easy to see that $\tilde{E}^z_{k10}$ is given by

$$\tilde{E}^z_{k10} = -i \left(\frac{4\rho^2 \cos\phi - w(z)^2 e^{-i\phi}}{Qkw(z)^4}\right) e^{-\frac{\rho^2}{w(z)^2} + i\Theta_{k10}} \quad (9)$$

The expression for $\tilde{E}^x_{k10}$ is obtainable in the same manner from Eqs. (1) and (2). Note that in the derivation leading to the closed analytical expression Eq.(6) for the longitudinal electric field we have kept the full z-dependence residing in $w(z)$ using the substitution $w(z) = \sqrt{2(z^2 + z_R^2)/kz_R}$ where $z_R = \pi w_0^2/\lambda = kw_0^2/2$ with λ the wavelength of the light. We have also taken full account of the convergence phases θ_{Gouy} and θ_{curve}. Similar evaluations for the case $\ell = -1$ have then been carried out straightforwardly, leading to the corresponding formalism for the doughnut beam with $\ell = -1$ for which the longitudinal electric field is $E^z_{k(-1)0}$.

It is interesting to consider the magnitude of the longitudinal field component E^z relative to that of the transverse component for the case $\ell = 1$ doughnut mode and make the comparison for different values of w_0 as shown in Fig. 1. The variations are evaluated in the focal plane for two sets of beam waists, w_0 large and w_0 small. It is clear from the plots that the longitudinal field is very small for larger w_0 relative to the corresponding transverse component, as in Fig.1(b). It becomes comparable to the transverse field for smaller w_0, as in Fig.1(a). It is also easy to deduce from the analytical expression for E^z in Eq.(6) on expanding the $\cos\phi$ in terms of exponentials we immediately see that this longitudinal field component is a superposition of the $\ell = 0$ mode and the $\ell = 2$ mode. It is clear then that it is the $\ell = 0$ mode that accounts for the central peak in Figs.1 (a) and (b).

The general definitions of the chirality and the helicity of a light field require, in addition to the usual electromagnetic fields, the introduction of dual fields. Accounts of optical chirality and helicity can be found in [19, 20] along with the recent literature on this subject. In the Coulomb gauge we have for the chirality

$$\chi = \frac{1}{2}\left(-\epsilon_0 \mathbf{E} \cdot \dot{\mathbf{B}} + \mathbf{B} \cdot \dot{\mathbf{D}}\right) \quad (10)$$

and for the helicity

$$\eta = \frac{1}{2}\left(\sqrt{\frac{\epsilon_0}{\mu_0}}\mathbf{A} \cdot \mathbf{B} - \sqrt{\frac{\mu_0}{\epsilon_0}}\mathbf{C} \cdot \mathbf{D}\right) \quad (11)$$

where $\mathbf{D} = \epsilon_0 \mathbf{E}$ is the displacement field while $\mathbf{C}$ is a second vector potential dual to the usual vector potential $\mathbf{A}$ such that $\boldsymbol{\nabla} \times \mathbf{C} = -\mathbf{D}$ and $\dot{\boldsymbol{C}} = -\mathbf{B}/\mu_0$. However, we will assume that we are dealing with cycle-averaged monochromatic fields in which case the cycle-averaged chirality $\bar{\chi}$ and the helicity $\bar{\eta}$ are given by

$$\bar{\chi} = -\frac{\omega\epsilon_0}{2}\Im[\mathbf{E}^* \cdot \mathbf{B}] = \frac{\omega^2}{c}\bar{\eta} \quad (12)$$

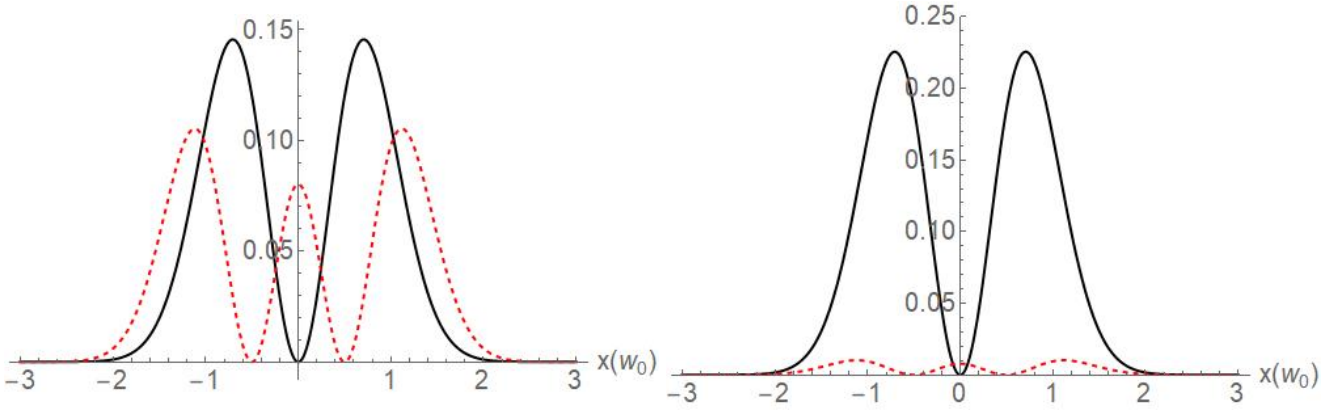

(a) $w_0 = 0.5\ \lambda$ (b) $w_0 = 2\ \lambda$

FIG. 1: The in-plane variations of the modulus squared of the electric field components for the $\ell = 1, p = 0$ Laguerre-Gaussian (doughnut) mode in the focal plane $z = 0$. The sub-figures compare the corresponding variations of the longitudinal field E^z (dotted red curve) with the transverse component E^x (solid black curve). (a) the case of a beam with a small beam waist $w_0 = 0.5\lambda$ where E^z is comparable with E^x and (b) the case of a relatively large beam waist $w_0 = 2\lambda$ where E^z appears negligibly small in comparison with E^x. These results also apply for the case $\ell = -1, p = 0$.

where $\Im$ stands for 'the imaginary part'. Thus in order to evaluate the helicity and the chirality we need to determine the magnetic field components using Maxwell's equation $\boldsymbol{\nabla} \times \mathbf{E} = i\omega\mathbf{B}$. There are three components of the magnetic field, given by

$$\mathbf{B} = \frac{1}{i\omega}\left\{\partial_y E^z \hat{\boldsymbol{x}} + (\partial_z E^x - \partial_x E^z)\hat{\boldsymbol{y}} - \partial_y E^x \hat{\boldsymbol{z}}\right\} \tag{13}$$

However, since $E^y = 0$, then as far as the evaluation of the dot product in Eq.(12) is concerned only the x and z components of the magnetic field are relevant and these are given by

$$B^x_{k10} = -\mathcal{U}_0 \frac{2\rho z_R \left(\sin 2\phi \left((3z_R - iz)\, w(z)^2 + 4i\rho^2 (z + iz_R)\right) + (z + 3iz_R)\, w(z)^2 \cos 2\phi - (z - iz_R)\, w(z)^2\right)}{\omega w(z)^6 (kz_R)^{3/2}} \times e^{-\frac{\rho^2}{w(z)^2} + i\Theta_{k10}} \tag{14}$$

$$B^z_{k10} = -\mathcal{U}_0 e^{-\frac{\rho^2}{w(z)^2}} e^{i\Theta_{k10}} \frac{-2iz_R w(z)^2 \sin(\phi) + 2z_R w(z)^2 \cos(\phi) + 4\rho^2 (z + iz_R)\sin(\phi)}{\omega w(z)^4 \sqrt{kz_R}} \tag{15}$$

Similar evaluations have been carried out straightforwardly for the magnetic field components in the case of $\ell = -1$. The results for the chirality distribution in the focal plane are shown in Fig.2 in which the two doughnut beams have the same waist $w_0 = 0.5\lambda$ and differ only in the sign of the winding number. Figure 2(a) concerns the doughnut beam with winding number $\ell = 1$ and 2(b) with negative winding number $\ell = -1$. The differences are clear in that regions of the focal plane where the chirality is high (bright red) in 2(b) are replaced by regions of low chirality density (in blue) in 2(a) and vise versa. The distributions cannot be described as mirror images of each other. These results confirm the chiral character of light carrying orbital angular momentum that is linearly polarised and so has no spin angular momentum. Figures 2(c) and 2(d) display the chirality distributions for the doughnut beams with much larger beam waist $w_0 = 5\lambda$ evaluated using the same paraxial formalism as for Figs 2(a) and 2(b). It is clear that the distributions are very similar to the small w_0 case in Figs. 2(a) and 2(b), with the only difference being that the magnitudes are much smaller. Thus we may infer that the preserva-

tion of the general features of the chirality and helicity for different w_0 is due to the topological nature of the doughnut beams.

Note that the assumption that we are dealing with cycle averaged fields meant that the helicity density is directly proportional to the chirality density, as described by Eq. (12).

The consideration so far have been concerned with the properties of the beams in the focal plane $z = 0$. It is, however, of interest to explore what changes occur in planes to the left $z < 0$ and to the right $z > 0$ of the focal plane to ascertain that the chirality features continue beyond the focal plane. The general expressions displayed above for the electric and magnetic fields show explicit spatial dependence on the axial and radial coordinates in both their amplitudes and phases, including those arising from the presence of the longitudinal field component. The convergence phase comprising the Gouy phase θ_{Gouy} and curvature phase θ_{curv} are both operative as displayed in Fig. 3 as well as the variations of $w(z)$. These phase functions can have relatively large gradients in the case of small beam waists in all planes in the vicinity of the focal plane.

Direct evaluations of the chirality distributions on the planes $z > 0 = +2w_0$ and $z < 0 = -2w_0$ (as done for the focal plane in Fig.2 a and b) leads to the rather different distributions shown in Fig.4. These results demonstrate that the topological chirality features exhibited in the focal plane still exist on both sides of the focal plane, but the distributions have evolved from their forms in the focal plane. In Figs.4 (a and b), which concern the plane $z = +2w_0$, the same chirality feature persists between the case $\ell = 1$ and the case $\ell = -1$ but both distributions are twisted by equal and opposite angles in comparison with the case in the focal plane in Figs.2(a) and 2(b). Figures 4(c and d) display the chirality distributions in the plane $z = -2w_0$ to the left of the focal plane and, once again, for $\ell = 1$ and $\ell = -1$. As before, there is a twist of the patterns relative to those in the focal plane, but the twisting is opposite to those for the same ℓ but on equidistant planes on different sides of the focal plane. In fact Fig. 4(a) and 4(d) show the same twist but reciprocal intensity distributions and the same features are displayed between Figs.4(b) and 4(c).

The chirality and the helicity of the LG beam we have focused on here are two of its main properties. We have shown that in the regime where the beams have small beam waist w_0, the longitudinal component of the electric field and its associated magnetic field become of the same order of magnitude as those of the corresponding transverse components. Such longitudinal components are very small and are normally discarded for beams with relatively large beam waist w_0. Our work has confirmed that light in the form of doughnut beams exhibits chirality in the sense that a change of the sign of the winding number ℓ produces a different chirality distribution. We have also shown that the convergence phases give rise to features additional to chirality in the vicinity of the focal plane in the form of a rotation of patterns and changes in equidistant planes on either sides of the focal plane.

The chiral nature of the LG light has been investigated experimentally by Wozniak et al [14] and their experimental findings were shown to conform with the results arising from the vectorial diffraction theory (see also [7] and references therein). The Wozniak et al's work had involved passing each doughnut beam through a lens and the chirality they measured was due to the fields observed in the back focal plane of this lens. With this arrangement they, too, confirmed the chiral character in the case of the two linearly polarized LG beams subject to focusing by the lens, one with winding number $\ell = 1$ and another with winding number $\ell = -1$ with neither beam possessing spin angular momentum. However, their chirality distribution in the back focal plane of the lens differs from our results which have been produced in the absence of a lens as shown in Figs. 2 and 4. We suggest that the differences lie in the manner in which the doughnut beams responded to the focusing lens in [14]. The changes could be related to the effect of the focusing of the linearly polarised vortex light, as pointed out in [2] and it has also been suggested that linearly polarised light falling onto the back focal plane of the lens becomes uniformly polarized [21]. These scenarios are not applicable to what we have been concerned with in this paper in which we have dealt with linearly-polarised doughnut beams with small w_0 and the chirality and helicity features we have confirmed are applicable to such beams subject to no further focusing by a lens as was the case investigated in [14].

To summarise, in this paper we have derived analytical expressions for the longitudinal electric field component and the corresponding magnetic field components for doughnut modes and shown that these are comparable in magnitude to the transverse components, but only for small w_0. We have also shown that substantial magnitudes of the chirality and helicity exist due to substantial longitudinal components and demonstrated explicitly the chirality distributions in the focal plane. Although the chirality density distributions are substantial for small beam waists, we have shown that the main features are independent of the beam waist, but the magnitudes become much smaller for larger beam waists. We have attributed this charcteritic feature to the topological nature of chirality. We have also explored the role of the Gouy and curvature phase gradients in the shape of the chirality density distributions on different sides of the focal plane. We have concentrated on generating figures mainly on cycle-averaged chirality density. This is because under such conditions, apart from a constant factor, the helicity distribution plots would look exactly the same as the chirality distributions. We have highlighted the interesting dual symmetry roles of the sign of

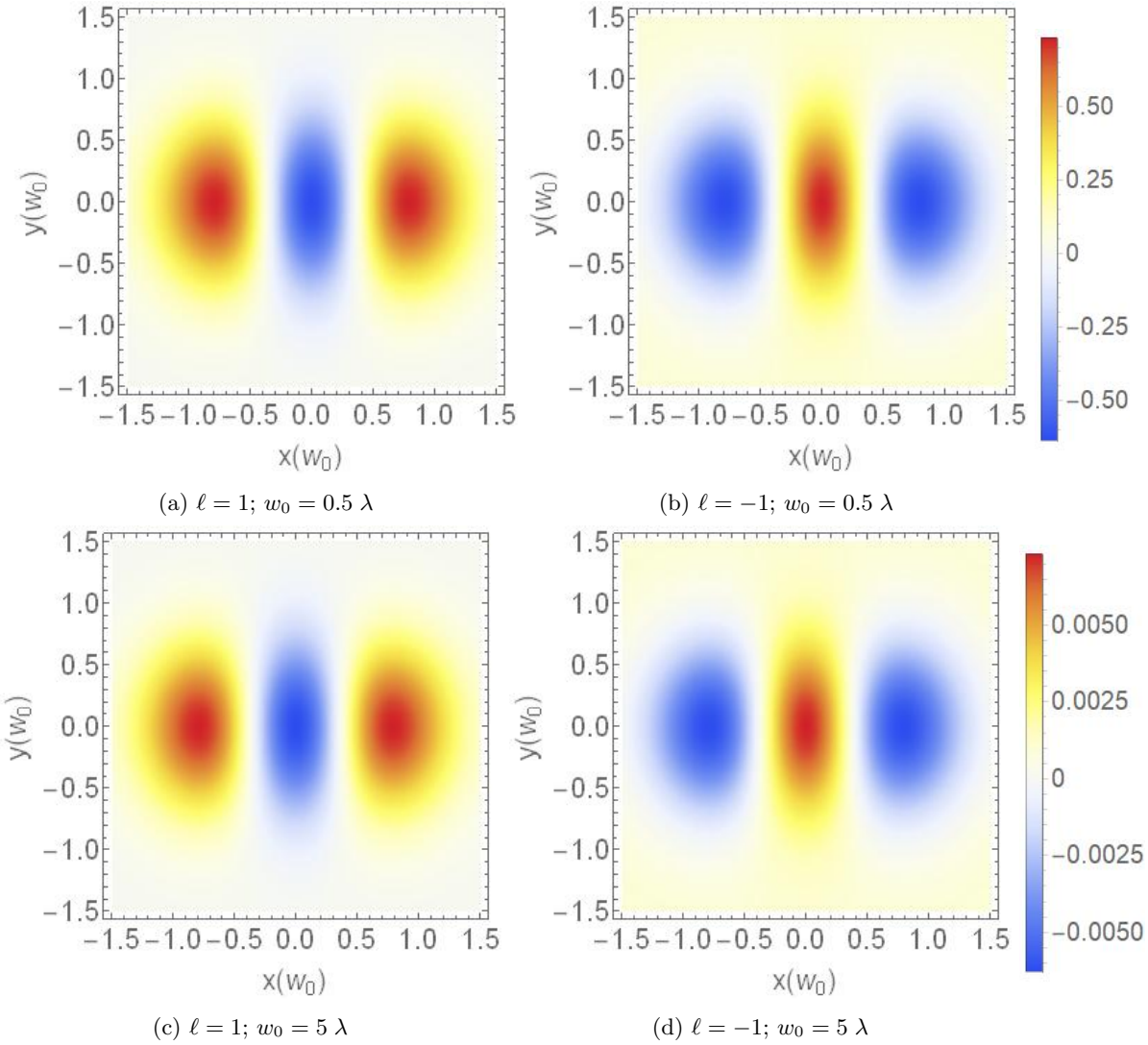

(a) $\ell = 1$; $w_0 = 0.5\ \lambda$

(b) $\ell = -1$; $w_0 = 0.5\ \lambda$

(c) $\ell = 1$; $w_0 = 5\ \lambda$

(d) $\ell = -1$; $w_0 = 5\ \lambda$

FIG. 2: The chirality distribution in the focal plane $z = 0$ for doughnut beams (a) and (b) which both have the same beam waist $w_0 = 0.5\lambda$, but in (a) the winding number is $\ell = 1$ while in (b) the winding number is $\ell = -1$. Figures 2(c) and (d) are as for (a) and (b), respectively, but in these the beam waist for both has the much larger value $w_0 = 5\lambda$. Thus increasing the beam waist makes no difference to the structure and appearance of the chirality density distribution, but the magnitudes are much smaller. This distinctive feature is attributable to the topological nature of the chirality.

the winding number and the sign of the plane side (to the left and right of the focal plane). We have explained the meaning of chirality in relation to Fig. 2 evaluated in the focal plane $z = 0$ where the Gouy and curvature phases vanish and so have no role to play as regards the chirality on the focal plane. We interpreted the interesting chirality shapes in Fig. 4 where $z \neq 0$ and emphasised the role played by the curvature and Gouy phases in the chirality distributions on planes to the left and to the right of the focal plane. We explained how changing the sign of the winding number and the signs of the left and right planes relative to the focal plane give rise to similarities and differences in the chirality distributions

We have been guided by the realisation that helicity and chirality are essentially topological properties of a light beam, which preserve their characters for beams with a given winding number, but different states of focusing. The paraxial formalism we have adopted in the paper stems directly from the fully non-paraxial formalism when the paraxial limit is taken. It is significant that the results of the chirality distributions in the case of large w_0 mirror those for the small w_0 case, but the magnitudes for the larger w_0 are very small, as expected. The paraxial regime does indeed describe, albeit largely qualitatively, the chirality and helicity of Laguerre-Gaussian beams. For larger w_0 the paraxial regime gives a reli-

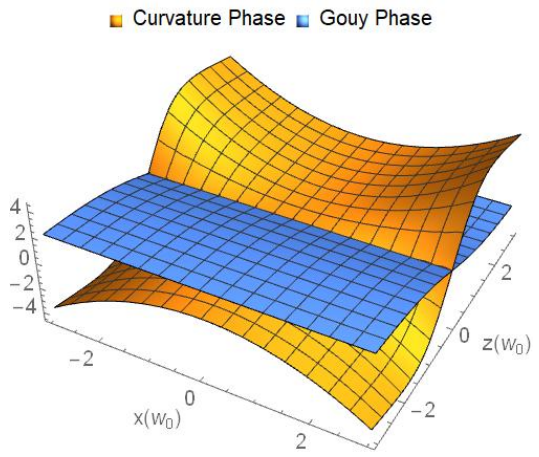

FIG. 3: Variations in the xz-plane of the Gouy phase θ_{Gouy} and the curvature phase θ_{curve} of the doughnut beam for which $w_0 = 0.5\lambda$. Note the sign change across the plane $z = 0$.

able indication of magnitudes as well, but the small w_0 case highlights both the appearance of a substantial longitudinal component and substantial magnitudes of the chirality and helicity distributions.

ACKNOWLEDGEMENTS

We are grateful to Professor S. M. Barnett for helpful discussions. KK wishes to thank Tubitak and Bitlis Eren University for financial support (under the project:BEBAP 2017.19) during his sabbatical year at the University of York where this work was initiated.

[1] R. Dorn, S. Quabis, and G. Leuchs, Physical Review Letters **91**, 1 (2003).
[2] R. Dorn, S. Quabis, and G. Leuchs, Journal of Modern Optics **50**, 1917 (2003), arXiv:0304001 [physics].
[3] T. Bauer, P. Banzer, E. Karimi, S. Orlov, A. Rubano, L. Marrucci, E. Santamato, R. W. Boyd, and G. Leuchs, Science **347**, 964 (2015).
[4] V. V. Kotlyar, S. S. Stafeev, and A. G. Nalimov, *Sharp Focusing of Laser Light* (CRC Press, 2019).
[5] S. Quabis, R. Dorn, M. Eberler, O. Glöckl, and G. Leuchs, Optics Communications **179**, 1 (2000).
[6] K. S. Youngworth and T. G. Brown, Opt. Express **7**, 77 (2000).
[7] Y. Zhao, J. S. Edgar, G. D. M. Jeffries, D. McGloin, and D. T. Chiu, Phys. Rev. Lett. **99**, 073901 (2007).
[8] Y. Tang and A. E. Cohen, Phys. Rev. Lett. **104**, 163901 (2010).
[9] A. Aiello, N. Lindlein, C. Marquardt, and G. Leuchs, Phys. Rev. Lett. **103**, 100401 (2009).
[10] P. Banzer, M. Neugebauer, A. Aiello, C. Marquardt, N. Lindlein, T. Bauer, and G. Leuchs, Journal of the European Optical Society - Rapid publications **8** (2013).
[11] A. Aiello, P. Banzer, M. Neugebauer, and G. Leuchs, Nature Photonics **9**, 789 (2015).
[12] K. Y. Bliokh and F. Nori, Physics Reports **592**, 1 (2015).
[13] G. F. Quinteiro, F. Schmidt-Kaler, and C. T. Schmiegelow, Phys. Rev. Lett. **119**, 253203 (2017).
[14] P. Woźniak, I. De Leon, K. Höflich, G. Leuchs, and P. Banzer, Optica **6**, 961 (2019).
[15] M. Babiker, D. L. Andrews, and V. E. Lembessis, Journal of Optics **21**, 013001 (2018).
[16] K. Koksal, V. E. Lembessis, J. Yuan, and M. Babiker, Journal of Optics **21**, 104002 (2019).
[17] M. Lax, W. H. Louisell, and W. B. McKnight, Phys. Rev. A **11**, 1365 (1975).
[18] S. M. Barnett and L. Allen, Optics Communications **110**, 670 (1994).
[19] F. Crimin, N. Mackinnon, J. Götte, and S. Barnett, Applied Sciences **9**, 828 (2019).
[20] F. Crimin, N. Mackinnon, J. Götte, and S. Barnett, Journal of Optics **21**, 094003 (2019).
[21] U. Levy, Y. Silberberg, and N. Davidson, Adv. Opt. Photon. **11**, 828 (2019).

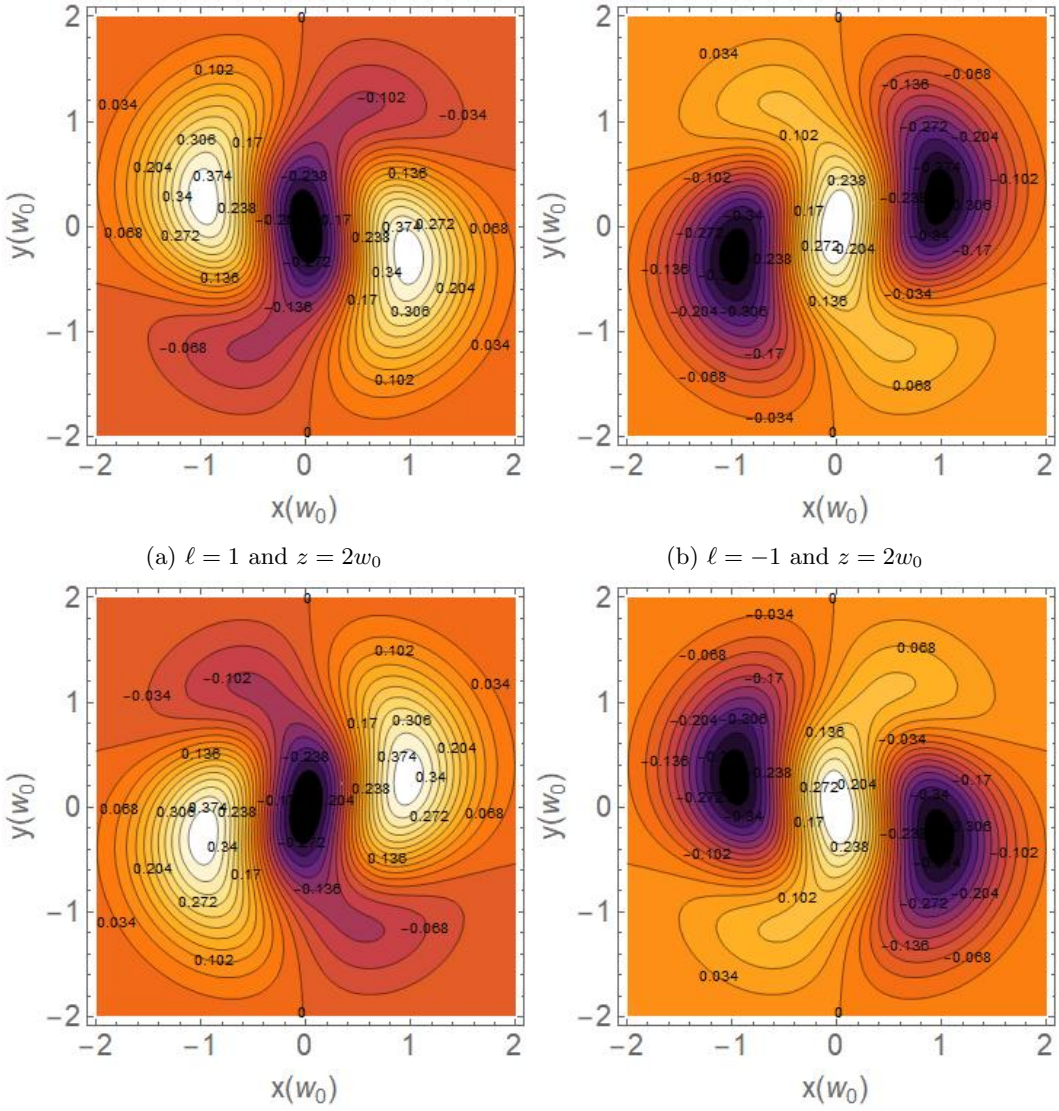

(a) $\ell = 1$ and $z = 2w_0$

(b) $\ell = -1$ and $z = 2w_0$

(c) $\ell = 1$ and $z = -2w_0$

(d) $\ell = -1$ and $z = -2w_0$

FIG. 4: The chirality distribution in the plane $z = +2w_0$ and $z = -2w_0$ in the vicinity of the focal plane for two doughnut beams for which the waist is $w_0 = 0.5\lambda$: Left panel (a and c): the case of a doughnut beam with winding number $\ell = 1$ (a) plane $z == +2w_0$ and (b) plane $z = -2w_0$. The right panel (b and d) is the same as the left panel, but for negative winding number $\ell = -1$.